Effects of geometrical parameter variations on the performance of silicon nitride-based optical microring resonators

H. HAROON[1,*], A. S. M ZAIN[1], S. K. IDRIS[1], H. A. RAZAK[1], M. OTHMAN[2], F. SALEHUDDIN[1]
[1]*Centre for Telecommunication Research and Innovation, Fakulti Teknologi dan Kejuruteraan Elektronik dan Komputer (FTKEK), Universiti Teknikal Malaysia Melaka (UTeM), Melaka, Malaysia*
[2]*Department of Electronic Engineering, Faculty of Electrical and Electronic Engineering, Universiti Tun Hussein Onn Malaysia, Batu Pahat, Malaysia*

This research proposes microring resonator (MRR) filter design based on silicon photonic technology on a silicon nitride (Si_3N_4) substrate for use as optical filters or passive wavelength filters in wavelength division multiplexing networks. Coupled mode theory and transfer matrix approaches were employed to investigate the effects of geometrical design variations on an optical filter model based on a Si_3N_4 MRR. Using MATLAB software, the geometrical parameters of a Si_3N_4 waveguide on silica were systematically analyzed and optimized. The four geometrical parameters studied to investigate changes in filter performance in terms of free spectral range and full wave half maximum were rib waveguide height, waveguide width, gap size, and ring radius. This work demonstrates the significance of selecting appropriate design parameters in the development of an optimal Si_3N_4-based MRR optical filter.

(Received March 6, 2023; accepted October 9, 2023)

Keywords: Microring resonators, Silicon nitride, Semiconductor design, Photonic device

1. Introduction

Optical fibers have largely replaced copper cables in key networks due to their numerous advantages over electricity transmission. High bandwidth, extremely low loss, wide transmission range, and the absence of electromagnetic interference, are all significant advantages of optical communication [1-4]. An optical communication system includes a modulator/demodulator, transmitter/receiver, light signal, transmission channel, and optical filter. Microring resonators (MRRs) are one of the optical components that are frequently used as a filtering function in dense wavelength division multiplexing (DWDM) communications, fabricated using photonic silicon technology [5-7]. An MRR is a set of waveguides comprising two straight waveguides and a ring waveguide. Microring resonators have recently gained recognition in DWDM applications due to superior characteristics, such as ultracompact size, simple design, and a wide range of tunability, making them suitable for optical filtering [8-10].

This paper investigates the design of a silicon nitride (Si_3N_4) MRR filter to address the issue of the passivation layer of photonic devices. Regardless of high temperatures, Si_3N_4 films are known to be excellent diffusion barriers for metal, water, and oxygen. Silicon nitride is also an ideal material for integrated photonic applications that use visible and near-infrared light. The material combines the transparency for visible and near-infrared wavelengths and is ideal for waveguides with low propagation loss (0.1 dB/cm–2 dB/m) [11,12].

Microring resonator filter design rules should account for single-mode waveguide design, a high-quality factor, the wide free spectral range (FSR) and full width at half maximum (FWHM) value, a high extinction ratio, and low power consumption. The quality factor of an MRR is inversely proportional to the FSR. Therefore, understanding how design parameter variation affects overall device performance is critical. The novelty of this research is the study of the effect of geometrical parameters on Si_3N_4-based MRR filter in terms of two main characteristics, FSR and FWHM [13,14].

The goal of this research is to propose design trade-offs for a SI_3N_4-based MRR optical filter suitable for WDM network applications. The guidelines described here can drive practical design to meet filtering requirements.

2. Device design

Fig. 1 depicts the proposed MRR's three-dimensional (3D) structure, which consists of a ring waveguide tightly coupled to two straight waveguides. The radius of the ring is denoted by *R*, and the gap between the straight and ring waveguides is denoted by *g*. In this study, the output power was monitored via the through and drop ports, while the input power was launched via the input port.

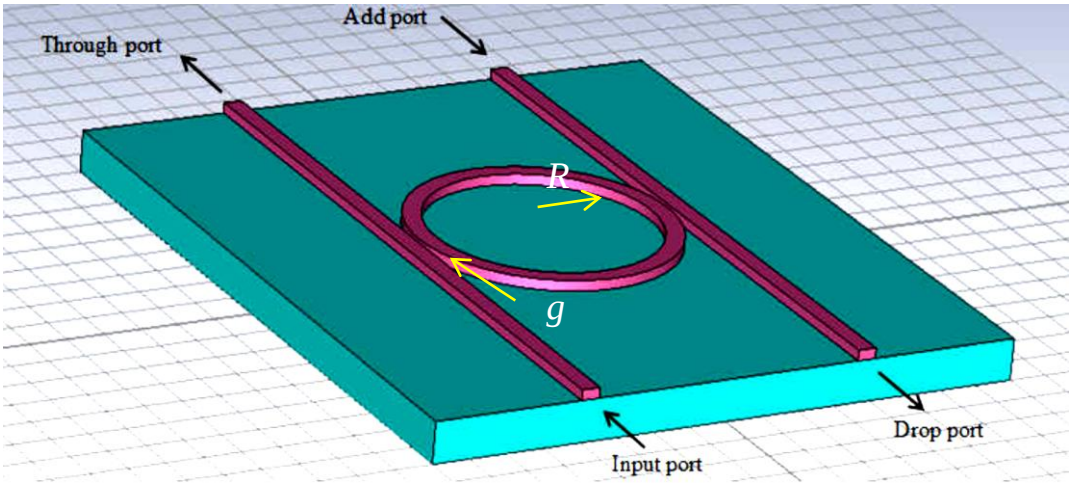

Fig. 1. The proposed MRR filter's 3D structure (color online)

The MRR device investigated in this study has a cross-section of 300 µm × 550 µm on top of a 1-m thick buried oxide SiO_2 layer, as shown in Fig. 2. From the diagram, the width of the waveguide is *W*, and the rib waveguide height is *H*.

Based on the resonance condition, the MRR will act as an optical filter that filters light waves at the desired wavelength. When light waves in the straight waveguide are in resonance with the ring, they are coupled into the cavity, then coupled out from the ring to the other straight waveguide, and finally exit at the drop port. In an off-resonance state, light waves bypass the ring and exit through the through port. The device's performance was evaluated by connecting TE light to the input port and scanning the output port response from 1.538 nm to 1.580 nm. In this study, the coupled mode theory (CMT) formulation is used to provide an analytical view of energy movement in the MRR, while the transfer matrix method (TMM) performs the coupled power transfer function between the straight and microring waveguides. The MRR modeling was carried out using MATLAB software, which can be referred from our previous study [14-15].

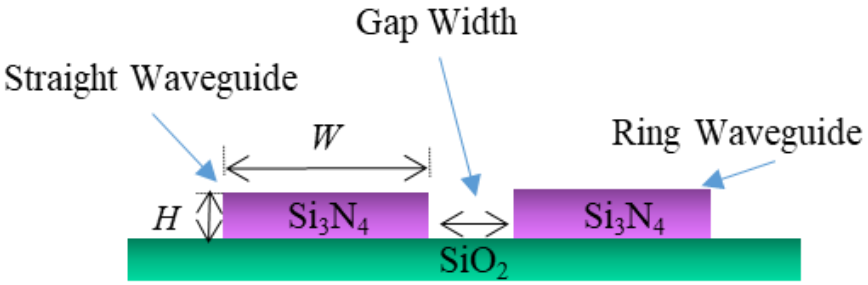

Fig. 2. Schematic cross-section of the rib waveguide MRR structure (color online)

The design of the filters for optical network applications should be primarily focused on the WDM network requirements (i.e., the pass bandwidth must be large enough to accommodate the entire signal spectrum). In addition, FSR and FWHM are the two parameters that must be emphasized to meet those requirements.

The FSR can be calculated by observing two consecutive peaks from the drop port spectral or by using the following equation [16]:

$$FSR = \frac{\lambda^2}{2\pi R n_g} \tag{1}$$

where n_g is the group index. A higher FSR indicates that more signals can be accommodated into the channel at the same time.

Another critical parameter is the resonance width, which is defined as the FWHM and can be expressed as follows [17]:

$$FHWM = \frac{k^2\lambda^2}{\pi L n_{eff}} \tag{2}$$

where n_{eff} is the effective refractive index, and *L* is the coupling length.

3. Results and discussion

The analysis was carried out by varying various critical design parameters to determine the effect of MRR performance based on a Si_3N_4 platform. These parameters include the gap separation between the straight bus and the ring (g), waveguide width (W), rib waveguide height (H), and ring radius (R). Table 1 summarizes the initial design specifications.

Fig. 3(a) depicts the mode profile of a nanometer-sized Si_3N_4 waveguide in the magnetic field component. Red represents high field intensity and turquoise blue represents low field intensity. It can be seen that the fundamental mode confines in the rib waveguide's core and partially overlaps in the sidewalls, inferring single-mode propagation. Fig. 3(b) depicts the MRR filter's response as monitored at the drop port, whereas Fig. 3(c) depicts the response as observed at the through port and the resonant peak indicates that the MRR is completely in resonant state. The through port's output is inversely proportional to the drop port's output. The resulting waveguide's effective index is 1.6858. From Fig. 3(b), the initial design has an FSR of 42.85 nm and a calculated FWHM of 1.74 nm.

Table 1. Initial design specifications

Parameter	Description	Value (unit)
n_2	n lower cladding	1.44
n_1	n core	1.996
n_o	n upper cladding	1
	Lower clad thickness	0.2 (μm)
H	Rib Waveguide Height	0.9 (μm)
	Upper Clad Thickness	0.5 (μm)
W	Waveguide width	0.8 (μm)
g	Separation Gap	0.1 (μm)
λ	Centre Wavelength	1.55 (μm)
R	Ring Radii	30 (μm)
k	Coupling Coefficient	0.01431
	Internal Loss	-3dB/cm

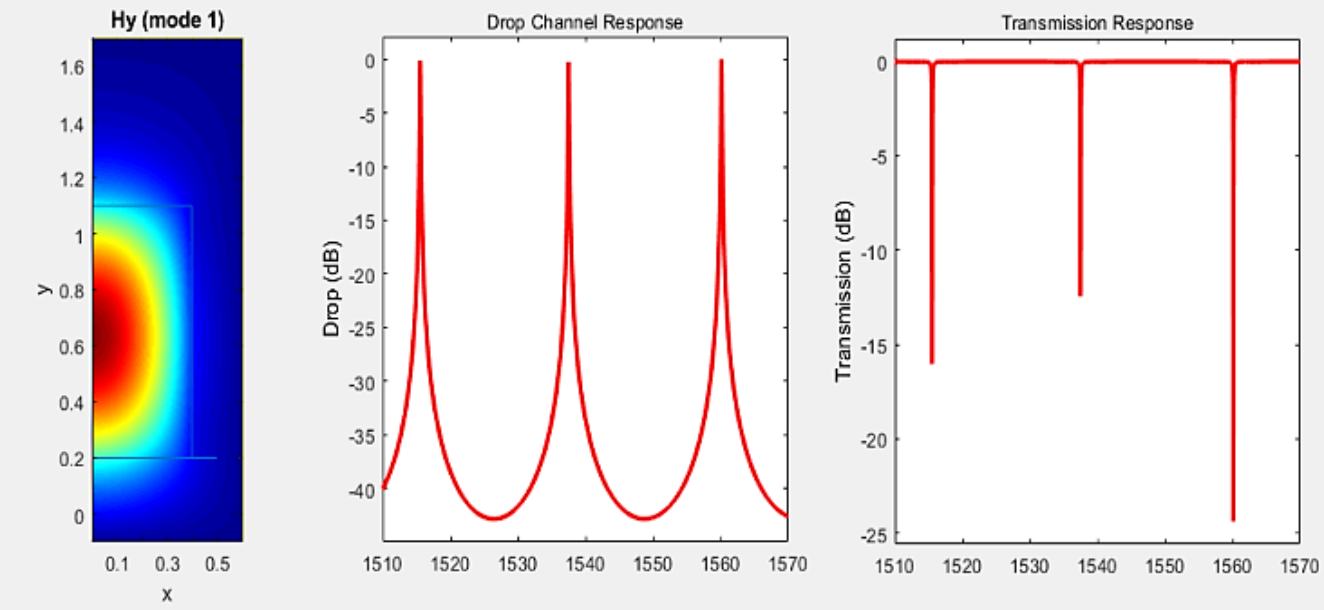

a) b) c)

Fig. 3. (a) MRR fundamental mode profile (b) Optical MRR Response at drop port (c) Optical MRR Response at through port (color online)

To investigate the impact of MRR radius on FSR and FWHM, device designs with radii ranging from 5 μm to 60 μm, with 5 μm increments, were modelled, and the results are shown in Fig. 4. Other parameters are left unchanged in this study, as in Table 1. It is apparent that both values decrease as the radius increases, implying that FSR and FWHM are inversely proportional to R. With ring radii of 5 μm, the highest FSR of 42.85 nm and FWHM of 1.7399 nm were obtained. In practice, compact MRR filter can only be realized with high-tech fabrication facilities. A relatively small R size also increases the device's sensitivity to fabrication tolerances. For comparison, [18] demonstrated an FSR of 0.9 nm for R=29 μm based on silicon on SiO_2 configuration. When compared to the closest radius in this study, which is 30 μm, the FSR value observed is 7.49 nm, indicating that the SI_3N_4 platform performs better in terms of FSR.

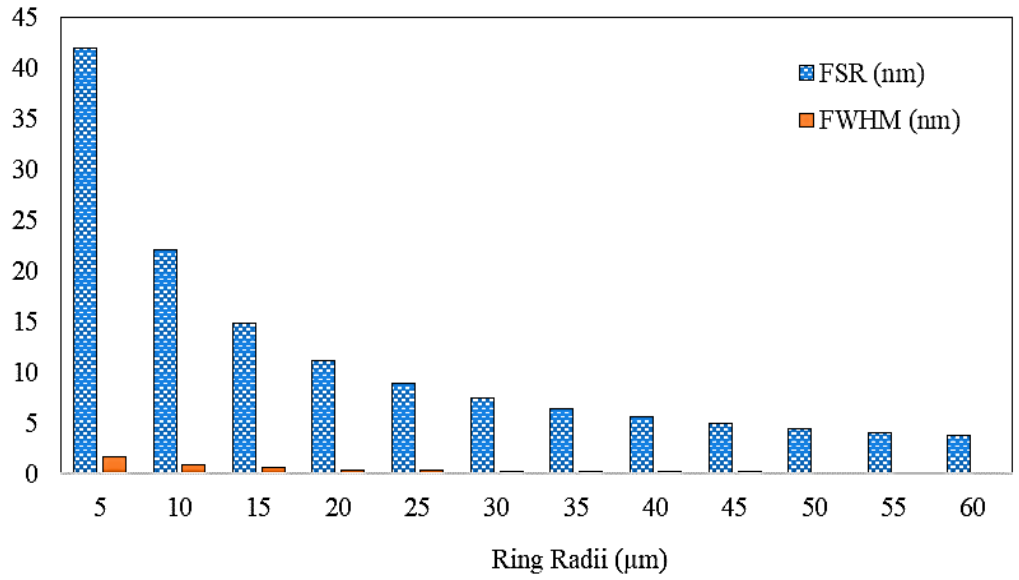

Fig. 4. Effect of ring radii variation on FSR and FWHM (color online)

The same approaches as in the previous procedure were pursued to investigate the effect of gap size on the FSR and FWHM, and the results are shown in Fig. 5. The FSR and FWHM decrease as the distance between the straight waveguide and the ring waveguide increases, indicating the same trend as the ring radii variation. The greater the distance between the two waveguides, the smaller the coupling coefficient, leading to high insertion loss at the output port. Indirectly, it will reduce FSR and FWHM. It is also worth noting that the intrinsic loss increases as the ring radii decrease, thereby increasing the device's extension ratio.

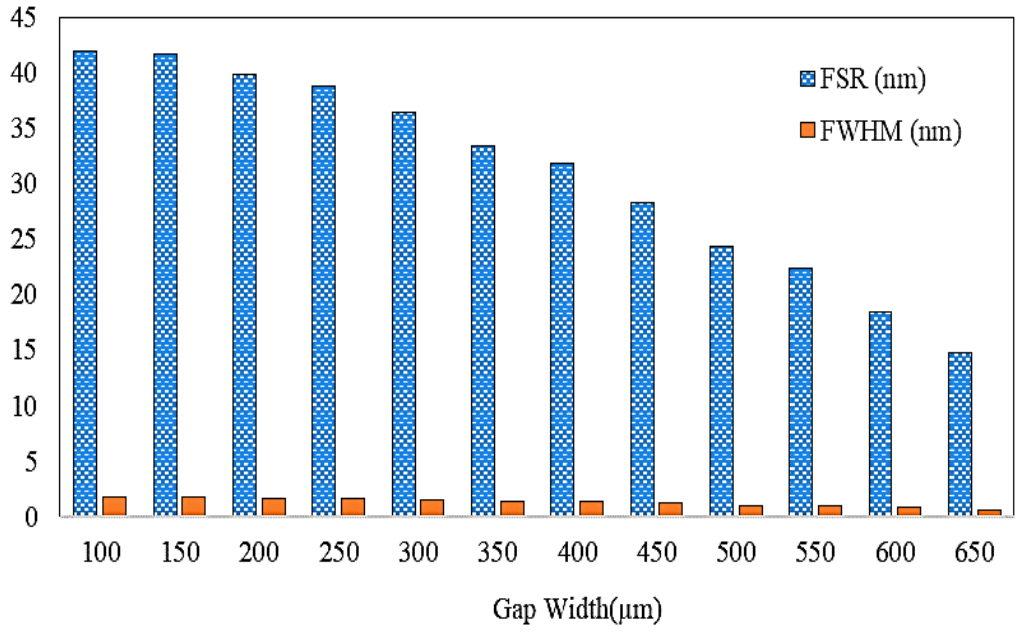

Fig. 5. Effect of gap width variation on FSR and FWHM (color online)

In addition to the radius and distance of the waveguide gap width, the width of the waveguide should also be considered when modeling the MRR filter. From Fig. 6, it is noticeable too that as the waveguide width increases, the FSR and FWHM decrease.

Given that there is less transient field overlap as the waveguide width increases, the coupling capability decreases, causing an increase in insertion loss and a decrease in FSR and FWHM.

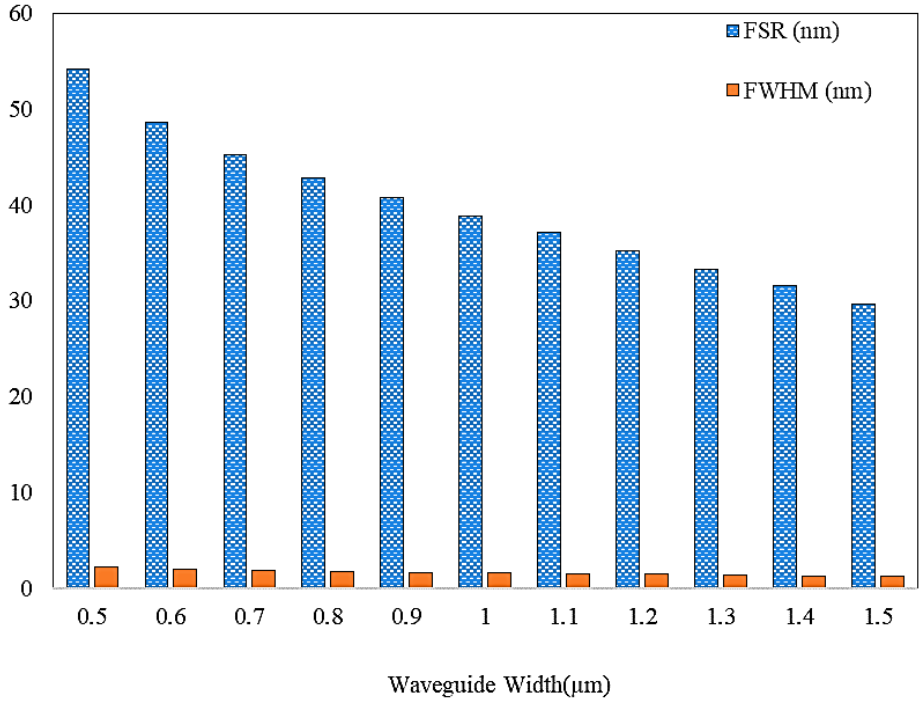

Fig. 6. Effect of waveguide width on FSR and FWHM (color online)

To study the impact of rib waveguide height on the FSR and FWHM, the rib waveguide height was varied from 0.5 to 1.5 μm. Fig. 7 shows that the FSR and FWHM decrease significantly between 0.5 and 1 μm. However, the FSR and FWHM remain after 1.1 μm, even after the rib height increases. Therefore, it can be concluded that a suitable rib height for the Si_3N_4 MRR design with other parameters set as in Table 1 is between 0.5 and 1.0 μm.

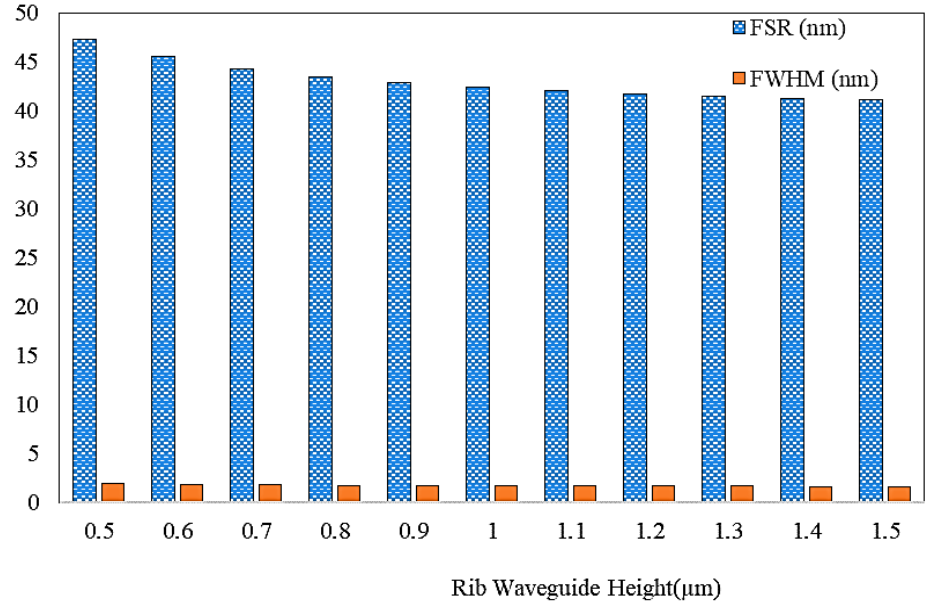

Fig. 7. Effect of rib waveguide height on FSR and FWHM (color online)

4. Conclusion

The influence of the MRR geometrical parameters (i.e., ring radius, rib waveguide height, waveguide width, and gap width) on the FSR and FWHM has been discussed. It can be concluded that the design parameters

play an important role in the development of a Si_3N_4-based MRR filter. The effect of waveguide geometry on filter performance has been investigated theoretically using CMT and TMM. Based on previous research, the obtained FSR and FWHM values meet the requirements of optical filter applications. It is also worth noting that, despite smaller optical filters have a good FSR and FWHM, very small devices are limited by fabrication tolerances. As a result, there must be design trade-offs when developing a high-performance optical filter. The findings of this study will provide useful guidance before any laboratory work is carried out for this purpose.

Acknowledgements

We would like to thank Universiti Teknikal Malaysia Melaka (UTeM) and the Ministry of Higher Education (MOHE). This research is supported by funding from MOHE via grant no. FRGS/1/2020/FKEKK-CETRI/F00429.

References

[1] T. Anbalagan, H. Haroon, H. A. Zain, H. Rafis, S. W. Harun, J. Eng. Sci. Technol. Rev. **15**(5), (2022).
[2] S. Kaur, P. Singh, V. Tripathi, R. Kau, Global Trans. Proc. **3**(1), 343 (2022).
[3] J. Ballato, Optics & Photonics News, **Mac** 2022.
[4] H. Haroon, A. Kareem, Optoelectron. Adv. Mat. **13**(5-6), 290 (2019).
[5] H. Hazura, A. R. Hanim Abdul, S. S. Khalid, N. Nadia, A. Aziz, Optoelectron. Adv. Mat. **11**(7-8), 393 (2017).
[6] B. Shi, X. Chen, Y. Cai, S. Zhang, T. Wang, Y. Wang, Sensors **22**(17), 6467 (2022).
[7] M. M. U. Hasan, M. S. Uddin, American Journal of Engineering Research **10**(7), 90 (2021).
[8] H. Haroon, S. Shaari, Menon, P. S. Menon, A. R. Hanim, B. Mardiana, Int. J. Numer. Model. El. **26**(6), 670 (2013).
[9] G. Chen, C. Jiang, Results in Phys. **19**, 103380 (2020).
[10] H. Sattari, A. Y. Takabayashi, P. Edinger, P. Verheyen, K. B. Gylfason, W. Bogaerts, N. Quack, J. Opt. Microsystems **2**(4), 044001 (2022).
[11] D. J. Blumenthal, R. Heideman, D. Geuzebroek, A. Leinse, C. Roeloffzen, Proc. IEEE **106**(12), 2209 (2018).
[12] C-P. Pedro, Photonics **9**(27), 1 (2022).
[13] G. M. Hasan, P. Liu, M. Hasan, H. Ghorbani, M. Rad, E. Bernier, T. J. Hall, Photonics **9**, 651 (2022).
[14] H. Hazura, P. S. Menon, B. Y. Majlis, A. R. Hanim, B. Mardiana, L. Hasanah, B. Mulyanti, D. Mahmudin, G. Wiranto, 10th IEEE Int. Conf. on Semiconductor Electronics (ICSE), 422 (2012).
[15] H. Haroon, S. Shaari, P. S. Menon, N. Arsad, A. R. Hanim, J. Telecommun. Electron. Comput. Eng. (JTEC) **7**(1), 31 (2015).
[16] S. Kisku, K. Sarwagya, S. Ranjan, Optical & Quantum Electronics **55**(2), 164 (2023).
[17] C. Julian, L. Hasanah, A. Aransa, R. Sumantri, H. S. Nugroho, A. Aminudin, S. K. Sahari, A. B. D. Nandiyanto, A. R. M. Zain, R. E. Pawinanto, B. Mulyanti, J. Eng. Sci. Technol. **15**(3), 1639 (2020).
[18] L. Zhang, L. Jie, M. Zhang, Y. Wang, Y. Xie, Y. Shi, D. Dai, Photonics Res. **8**, 684 (2020).

*Corresponding author: hazura@utem.edu.my